Neuron
NeuroResource

Chemogenetic Synaptic Silencing of Neural Circuits Localizes a Hypothalamus → Midbrain Pathway for Feeding Behavior

Tevye J. Stachniak,[1,2] Anirvan Ghosh,[2,3] and Scott M. Sternson[1,*]
[1]Janelia Farm Research Campus, HHMI, 19700 Helix Drive, Ashburn, VA 20147, USA
[2]Neurobiology Section, Division of Biological Sciences, University of California, San Diego, La Jolla, CA 92093, USA
[3]Neuroscience Discovery and Translation Area, Pharma Research and Development, F. Hoffmann-La Roche, 4070 Basel, Switzerland
*Correspondence: sternsons@janelia.hhmi.org
http://dx.doi.org/10.1016/j.neuron.2014.04.008

SUMMARY

Brain function is mediated by neural circuit connectivity, and elucidating the role of connections is aided by techniques to block their output. We developed cell-type-selective, reversible synaptic inhibition tools for mammalian neural circuits by leveraging G protein signaling pathways to suppress synaptic vesicle release. Here, we find that the pharmacologically selective designer G_i-protein-coupled receptor hM4D is a presynaptic silencer in the presence of its cognate ligand clozapine-*N*-oxide (CNO). Activation of hM4D signaling sharply reduced synaptic release probability and synaptic current amplitude. To demonstrate the utility of this tool for neural circuit perturbations, we developed an axon-selective hM4D-neurexin variant and used spatially targeted intracranial CNO injections to localize circuit connections from the hypothalamus to the midbrain responsible for feeding behavior. This synaptic silencing approach is broadly applicable for cell-type-specific and axon projection-selective functional analysis of diverse neural circuits.

INTRODUCTION

Rapid, reversible, and cell-type-specific blockade of synaptic communication between neurons is important for assessing the function of circuit connections. Several genetically encoded tools have been developed for inhibiting synaptic vesicle release. For example, temperature-sensitive impairment of synaptic transmission with *shibire*^{ts}, a dynamin allele, has been widely used in *Drosophila* behavioral studies to provide rapid and reversible inhibition of genetically defined circuits (Kitamoto, 2002). Likewise, blockade of synaptic transmission with tetanus toxin light chain has been refined to allow inducible blockade, albeit over slow timescales of days to weeks, through doxycycline-dependent control of tetanus toxin light chain expression (Yamamoto et al., 2003). However, neither of these methods provides a means to spatially restrict synaptic inhibition to just a subset of neuronal projections originating from a cell type. MIST is a chemogenetic method for inactivating synaptic release in the presence of a small molecule, but it requires considerable overexpression to overcome endogenous synaptic release machinery (Karpova et al., 2005). InSynC, an optogenetic method, reduces evoked synaptic release in the presence of blue light by chromophore-assisted light inactivation of synaptic vesicle proteins, but this is accompanied by an undesirable rise in spontaneous neurotransmitter release (Lin et al., 2013). Other cell-type-specific methods for blocking circuit connections such as optogenetic (Stuber et al., 2011; Tye et al., 2011) or chemogenetic (Magnus et al., 2011) silencing of axon projections are not restricted to blocking local synaptic function and could also block action potential transmission in axons expressing the silencers that pass through the targeted site to more distal brain regions, essentially analogous to a cell-type-selective "reversible knife cut."

We considered pharmacological methods to achieve rapid, reversible, selective, and localized control over synaptic vesicle release. Metabotropic signaling from G_i-coupled receptors, for example, $GABA_B$ receptors or opioid receptors, are well established to suppress synaptic vesicle release (Heinke et al., 2011; Takahashi et al., 1998). Multiple mechanisms appear to be involved (de Jong and Verhage, 2009; Dittman and Regehr, 1996), including calcium channel suppression (Hescheler et al., 1987; Takahashi et al., 1998) and interference with the synaptic vesicle fusion machinery (Blackmer et al., 2001; Photowala et al., 2006). To achieve cell-type-specific metabotropic control over similar pathways, we considered the possibility that a chemogenetic G_i-coupled signaling pathway would possess synaptic silencing activity that could be targeted using genetic methods and activated pharmacologically. The designer receptor hM4D is a modified version of the G_i-coupled human muscarinic receptor 4 that responds to the highly selective exogenous ligand clozapine-*N*-oxide (CNO) and has been reported to inhibit neuron electrical activity (Armbruster et al., 2007). In addition, the native muscarinic 4 receptor is present in presynaptic terminals (Rouse et al., 1998) and has been demonstrated to suppress synaptic transmission (Dolezal and Tucek, 1998; Zhang et al., 2002). Moreover, hM4D/CNO has been noted to reduce an evoked synaptic current amplitude (Bock et al., 2013) and also reduces spontaneous synaptic release frequency (Mahler et al., 2014). However, neither of these studies determined

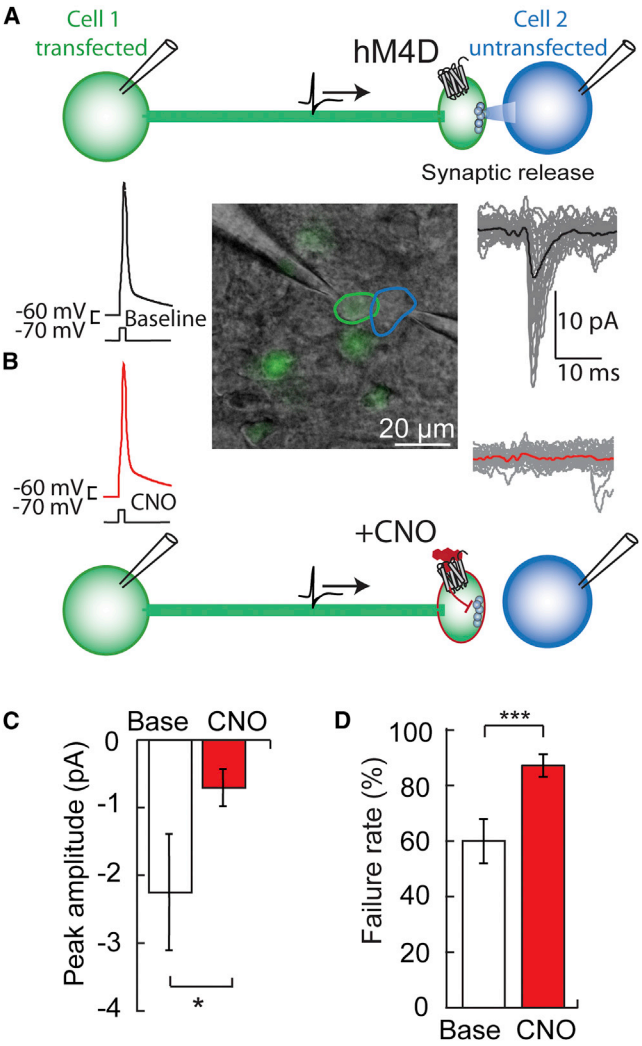

Figure 1. hM4D Is a Synaptic Silencer

(A) In paired whole-cell patch-clamp recordings of an hM4D-expressing presynaptic neuron (green) and an untransfected postsynaptic neuron (blue), action potentials elicited by current injection (1.5 nA) in the presynaptic cell produce excitatory synaptic currents in the postsynaptic partner.

(B) In the presence of the hM4D agonist CNO, the presynaptic action potential is still elicited, but postsynaptic currents are inhibited.

(C) The average peak amplitude of the postsynaptic current (Base) is reduced with CNO (n = 6).

(D) Failure rate increases with CNO, indicating a reduction in presynaptic release probability (n = 6). Values are represented as means ± SEM. *p < 0.05, ***p < 0.001.

whether hM4D acts explicitly to suppress neurotransmitter release probability as opposed to the potential effects of hM4D signaling on axonal excitability. Here, we show that hM4D and an axon-selective variant are cell-type-specific and projection-selective synaptic silencers when engaged by CNO and that this activity is independent of the influence of hM4D on neuron excitability. We also performed in vivo calibration for intracranial microinjections of the ligand CNO for spatially precise suppression of circuit connections. We applied this tool for functional analysis of a hypothalamic feeding circuit, which enabled identification of a hypothalamus→midbrain feeding pathway.

RESULTS

hM4D Is a Synaptic Silencer

We assessed the synaptic silencing capabilities of hM4D in pairs of synaptically connected layer 2/3 (L2/3) cortical neurons. Injection of depolarizing current triggered action potentials in hM4D-expressing presynaptic neurons, which resulted in evoked synaptic currents in their postsynaptic partners (Figure 1A). The modest hyperpolarization of presynaptic hM4D-expressing L2/3 neurons exposed to CNO (ΔV_m, −2.5 ± 0.6 mV; 30 nM CNO; p = 0.003 paired t test, n = 8; Figure S1A available online) did not prevent action potential initiation in the presynaptic neuron during current injection through the patch pipette. Application of CNO reliably suppressed synaptic transmission (peak current: −2.3 ± 0.9 pA; with 0.03–1 μM CNO: −0.7 ± 0.3 pA; p = 0.03, paired t test, n = 6) (Figures 1B and 1C). Synaptic suppression corresponded to an increased synaptic failure rate, i.e., the frequency with which a presynaptic action potential failed to generate a postsynaptic current (failure rate, baseline: 60.0% ± 7.9%; CNO: 87.2% ± 4.1%; p < 0.001, paired t test, n = 6) (Figure 1D). Input resistance in the postsynaptic cell, which lacked hM4D, was not significantly altered by exposure to CNO (baseline: 286 ± 50 MΩ; CNO: 257 ± 35 MΩ; p = 0.2, paired t test, n = 6). Therefore, the reduced amplitude of synaptic currents and the increase in synaptic failure rate, which provides a direct measure of presynaptic release probability (Dobrunz and Stevens, 1997), demonstrates that hM4D signaling can robustly inhibit synaptic neurotransmitter release.

We further investigated synaptic silencing with hM4D/CNO in axonal projections from L2/3 to cortical layer 5 (L5). For this, we coexpressed channelrhodopsin-2 (ChR2) in L2/3 neurons along with hM4D using a *Thosea asigna* virus 2a (Donnelly et al., 2001) ribosomal skip sequence (ChR2-2a-hM4D). This configuration allowed us to use laser-scanning photostimulation to rapidly probe connection properties of hM4D-expressing presynaptic neurons. It was important to determine a photostimulation intensity that overcame the modest hyperpolarization generated by hM4D activation (ΔV_m, −5.0 ± 0.7 mV; 1 μM CNO; p < 0.001, paired t test versus baseline, n = 7), and action potentials in L2/3 neurons could be reliably evoked with perisomatic photostimulation in the presence of 1 μM CNO (action potential fidelity, baseline: 93.1% ± 3.3%; CNO: 92.7% ± 3.4%; p = 0.5, paired t test, n = 11) or 10 μM CNO (action potential fidelity, baseline: 97.7% ± 1.7%; CNO: 94.8% ± 2.5%; p = 0.09, paired t test, n = 12) (Figures 2A and 2C). Postsynaptic currents in L5 cortical neurons were evoked by targeted photostimulation of L2/3 somata, and light-evoked synaptic currents were greatly reduced (88%) with CNO (1 μM) (peak current, baseline: 19.1 ± 4.6 pA; CNO: 2.2 ± 0.5 pA; p = 0.004, paired t test, n = 7) (Figure 2B). This effect on synaptic transmission occurred within minutes and washed out slowly, after which the synapse was sensitive to resilencing by CNO (Figures S1B and S1C). The IC_{50} for synaptic inhibition with CNO was 0.03 μM (Figure 2C), similar to the reported dose response for CNO activation of the related receptor hM3D (Armbruster et al., 2007). As expected

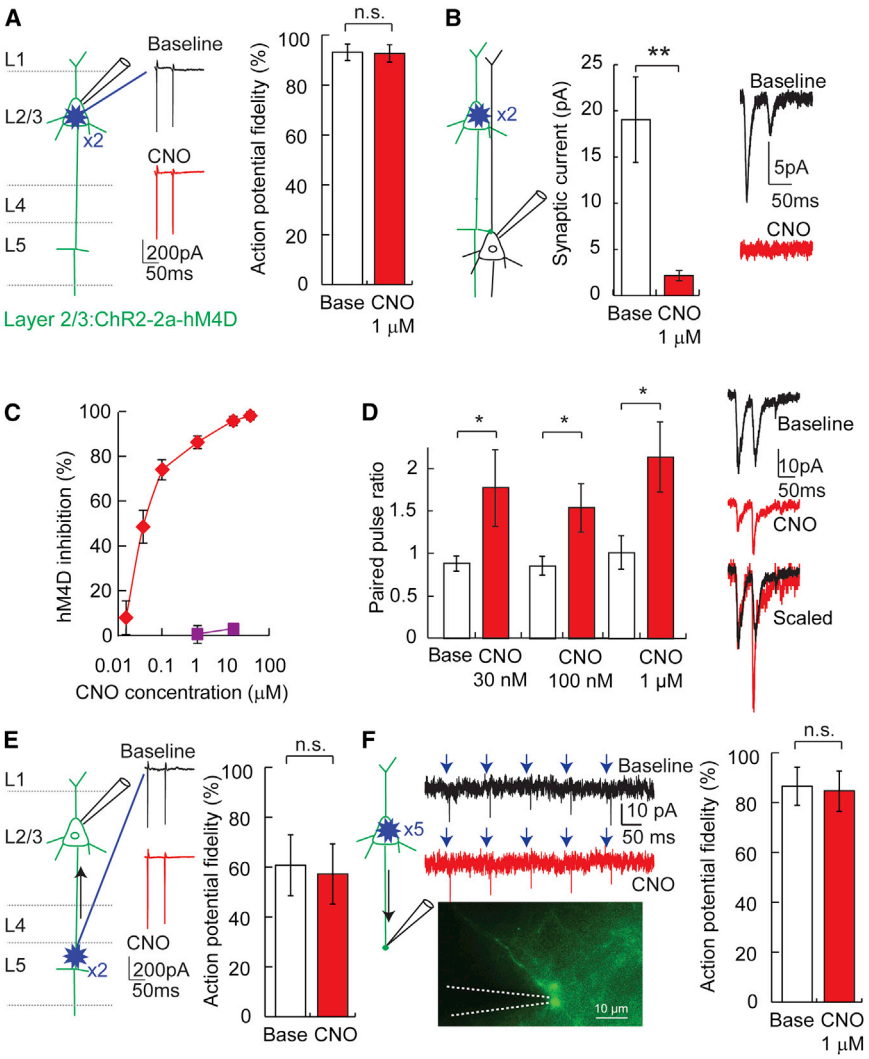

Figure 2. Efficacy and Potency of hM4D/CNO Synaptic Silencing

(A) During loose-seal cell-attached recordings in brain slices, pairs of photostimuli were targeted with a focal laser spot (blue starburst) to ChR2/hM4D-transfected L2/3 neurons, which evoked action potentials from somata in L2/3. Application of CNO (1 μM) does not substantially inhibit the fidelity (action potential/photostimulus) of ChR2-evoked action potential initiation.

(B) In whole-cell recordings from postsynaptic L5 neurons, CNO (1 μM) inhibits synaptic currents evoked by photostimulation of presynaptic L2/3 neuron somata (n = 7) with two light pulses.

(C) CNO potently inhibits synaptic transmission (red diamonds) but does not impair ChR2-induced action potentials (purple squares).

(D) Paired-pulse photostimulation of ChR2/hM4D-expressing L2/3 neurons (2 × 1 ms, 20 Hz) showed increased paired-pulse ratio (P_2/P_1) for evoked synaptic currents in L5 neurons (30 nM, 100 nM, and 1 μM CNO; n = 8, 6, and 7, respectively), indicating that hM4D/CNO reduces presynaptic release probability.

(E) Cell-attached recordings of back-propagating action potentials elicited by photostimulation of L2/3→L5 axons in L5 (blue starburst). L2/3 neurons coexpressed ChR2 and hM4D. Application of CNO (1–10 μM) did not reduce the fidelity of action potential back propagation (n = 8).

(F) In axon-attached recordings from the cut ends of L2/3 neuron-transfected axons in L4 and L5, axonal action potentials arising from L2/3 somatic photostimulation were not impaired by hM4D/CNO signaling, demonstrating that hM4D does not suppress action potential propagation. Values are represented as means ± SEM; n.s. $p > 0.05$, *$p < 0.05$, **$p < 0.01$.

for presynaptic inhibition (Zucker and Regehr, 2002), the reduction in synaptic transmission was accompanied by an increased paired-pulse ratio during exposure to several CNO concentrations (Figure 2D). These experiments show that, for an afferent axon projection pathway, hM4D/CNO is a potent, rapidly acting, and reversible synaptic silencing system.

Because our aim was to develop a selective synaptic silencer for neural circuits, we wanted to examine whether hM4D/CNO might undesirably also act by suppressing action potential propagation along axons. We determined that action potential backpropagation was unaffected in L2/3→L5 axon projections by photostimulation of axons in L5, which were still detected at the somata of hM4D-expressing L2/3 neurons in CNO (action potential fidelity, baseline 60.6% ± 12.2%; 1–10 μM CNO: 57.1% ± 12.1%; p = 0.2, paired t test, n = 8) (Figure 2E). In addition, loose-seal axon-attached recordings from L2/3 neuron cut axons in layers 4 or 5 showed no significant impairment of light-activated action potentials initiated at L2/3 somata (action potential fidelity, baseline: 86.5% ± 7.6%; CNO 1 μM: 84.6% ± 8.1%; p = 0.2, paired t test, n = 8) (Figure 2F). These experiments demonstrate that hM4D/CNO can selectively silence synaptic transmission without blocking axonal action potential propagation.

Suppression of Synaptic Release In Vivo

We next applied hM4D/CNO to inhibit synaptic release from a molecularly defined circuit in vivo using intracranial microinjection of CNO to discrete brain areas. A critical consideration was to identify the lowest efficacious dose of CNO for in vivo microinjection, in order to optimize the spatial resolution of projection field silencing by avoiding hM4D activation at sites distant from the targeted region due to spread of the agonist. Therefore, we calibrated the CNO dose for synaptic inhibition by monitoring the behavioral output from a previously characterized (Atasoy et al., 2012) hypothalamic circuit projection between molecularly defined AGRP neurons in the hypothalamic arcuate nucleus (ARC) and paraventricular hypothalamic (PVH) neurons (ARC^{AGRP}→PVH) (Figure S2A). Activation of AGRP neurons is sufficient to rapidly elicit avid food intake (Aponte et al., 2011) through axonal release of GABA and NPY in multiple brain areas

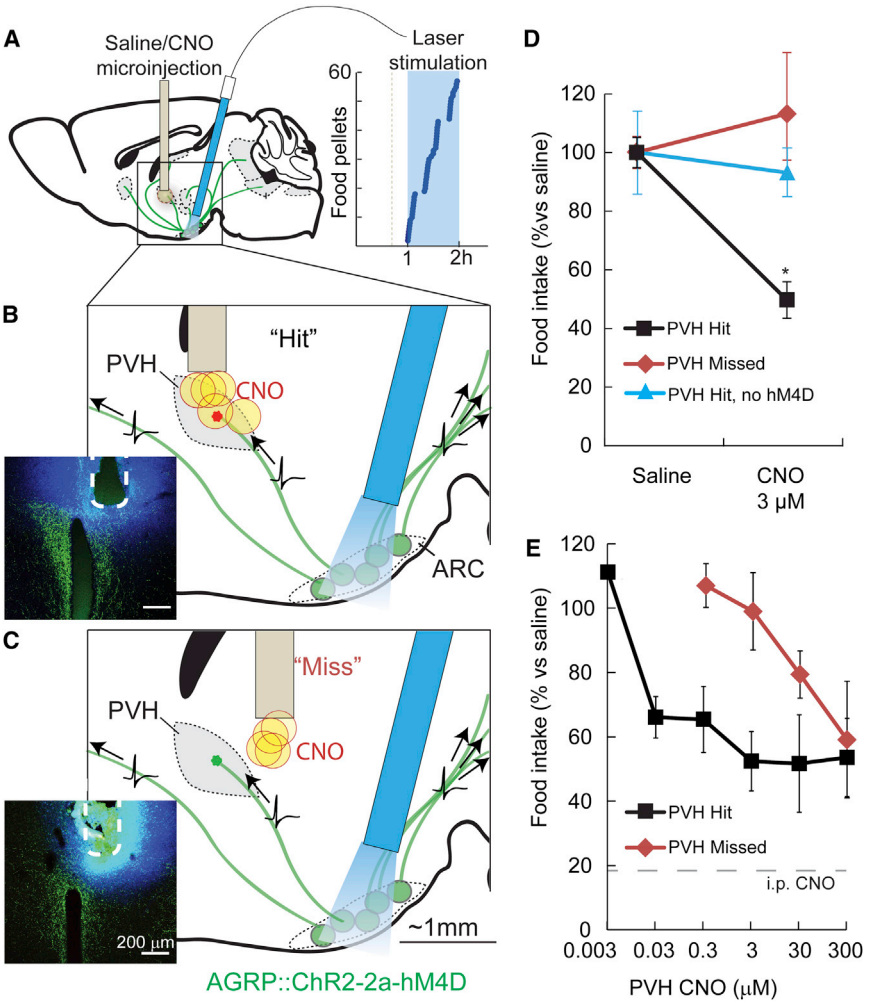

Figure 3. Spatially Targeted Synaptic Silencing In Vivo

(A–C) Schematics for photostimulation of AGRP neurons coexpressing ChR2 and hM4D in the arcuate nucleus (ARC), while spatially targeting CNO microinjection to the PVH. An angled optical fiber is implanted over the ARC to photostimulate AGRP neuron somata (green), which project axons to multiple brain areas. AGRP neuron photostimulation in this configuration robustly evoked feeding (right). CNO or saline were targeted to the PVH through an implanted cannula. (B) Focal microinjection of CNO to the PVH during AGRP neuron photoactivation result in selective silencing of synaptic release from the targeted ARC^{AGRP}→PVH axonal projection field due to hM4D-mediated synaptic inhibition. Evoked food intake is only partially reduced because AGRP neuron axons still transmit action potentials, and nontargeted axon projections remain competent for synaptic transmission. Injection sites were verified postmortem (inset) by injection of FluoroGold (blue) and AGRP immunofluorescence (green). (C) In some mice, cannula placement was outside of the PVH by 300–500 μm ("Miss").

(D) Local microinjections of CNO into the PVH ("Hits") significantly reduced feeding (3 μM CNO, n = 5). No reduction in feeding was observed for CNO injections that missed the PVH (3 μM CNO, n = 4) or with CNO injections into ChR2-expressing mice that lack hM4D (300 μM CNO, n = 5).

(E) PVH microinjection of CNO reduced feeding by about 50% over a range of doses. Precision of targeted synaptic silencing was reduced with increasing CNO dose, as evidenced by the capacity of injections that miss the PVH to inhibit feeding. Intraperitoneal injection of CNO further reduced evoked feeding to basal levels (18% ± 4% of evoked feeding). Values are represented as means ± SEM. *p < 0.05.

(Figure S2A). Prior work using pharmacological methods for blocking GABA or NPY receptor signaling in the PVH during AGRP neuron activation found that blockade of this circuit suppresses evoked feeding by ~50% (Atasoy et al., 2012). Therefore, we used hM4D/CNO to inhibit synaptic release from ARC^{AGRP}→PVH axons, which allowed us to use the reduction of evoked food consumption as a readout for the efficacy of in vivo cell-type-specific synaptic silencing.

To selectively block ARC^{AGRP}→PVH circuits with hM4D/CNO, we first determined ex vivo that hM4D signaling robustly suppressed ChR2-evoked synaptic transmission in ARC^{AGRP}→PVH circuits, which was reduced by 84% (peak current, baseline: 12.1 ± 3.2 pA; CNO: 1.9 ± 0.6 pA; p = 0.01, paired t test, n = 5) (Figure S2B). As demonstrated previously (Krashes et al., 2011), hM4D also decreased spontaneous firing in AGRP neurons (baseline firing rate: 1.91 ± 0.51 Hz; 1 μM CNO: 0.77 ± 0.48 Hz; p = 0.04, paired t test, n = 7); however, light-evoked action potential fidelity in ChR2/hM4D coexpressing AGRP neurons was not significantly reduced in the presence of CNO (baseline: 97.6% ± 1.7%; CNO 1 μM: 92.4% ± 4.6%; p = 0.1, paired t test, n = 7). For in vivo analysis, mice coexpressing ChR2 and hM4D in AGRP neurons were implanted with an optical fiber positioned to evoke feeding by photostimulating AGRP somata in the ARC (1 hr), along with a microinjection cannula above the PVH (Figure 3A). Intracranial microinjection of CNO (3 μM, 50–100 nl) in the PVH reduced feeding by ~50% during AGRP neuron photostimulation (PVH saline: 0.65 ± 0.17 g; PVH CNO: 0.32 ± 0.04 g; p = 0.01, paired t test, n = 5) (Figures 3B and 3D), similar to previous results using pharmacological blockade of GABA receptors and NPY1R in the PVH (Atasoy et al., 2012). In control animals transfected with ChR2 but not hM4D, CNO injection to the PVH did not reduce evoked feeding even at the highest CNO doses tested (PVH saline: 0.91 ± 0.13 g; CNO 300 μM: 0.84 ± 0.07 g; p = 0.2, paired t test, n = 5) (Figure 3D). Furthermore, synaptic inhibition with CNO was spatially localized to the PVH, because microinjections that missed the PVH by 300–500 μm (3 μM CNO, 50–100 nl) did not impair AGRP neuron-evoked feeding (saline: 0.46 ± 0.03 g; CNO: 0.52 ± 0.10 g; p = 0.3, paired t test, n = 4) (Figures 3C and 3D). At higher CNO doses, feeding suppression did occur with the mistargeted microinjections, indicating substantially reduced precision (Figure 3E). Thus by establishing an in vivo dose response

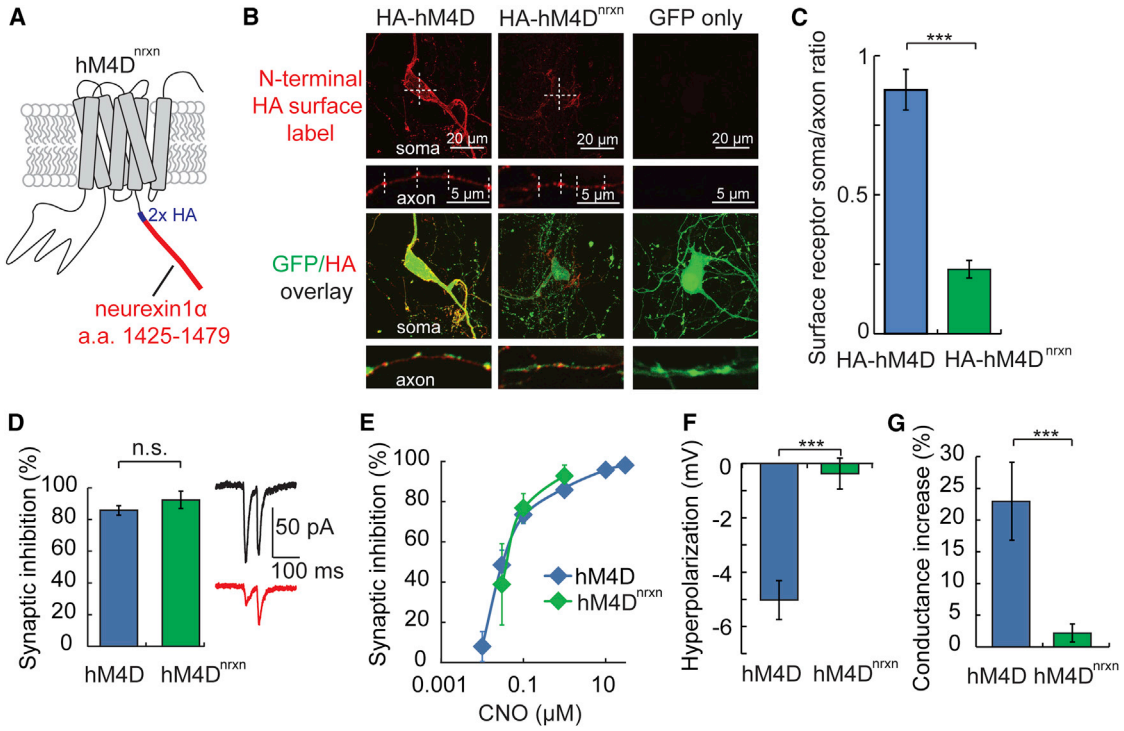

Figure 4. Axon Projection-Selective Silencing with hM4D^{nrxn}

(A) hM4D^{nrxn} was constructed by addition of an intracellular amino acid sequence from neurexin-1 (aa 1,425–1,479) to the C terminus of hM4D that also contained a C-terminal hemagglutinin (HA) tag.

(B) Cell surface distribution of N-terminal (extracellular) epitope-tagged HA-hM4D (Armbruster et al., 2007) and HA-hM4D^{nrxn} (see Experimental Procedures) was determined in hippocampal neuronal cultures that were cotransfected with EGFP. For surface labeling, anti-HA immunofluorescence was measured without membrane permeabilization. HA-hM4D^{nrxn} showed reduced intensity in the somatic compartment but not the axonal compartment, compared to HA-hM4D. Label intensity was quantified using linescans (hashed lines) across the cell body or synaptic boutons. EGFP fluorescence (HA/EGFP overlay) was used to trace axons and identify transfected neurons. Representative soma and axon images of anti-HA immunofluorescence were adjusted identically for brightness and contrast for display purposes. Cells transfected with EGFP alone did not show detectable signal for surface label anti-HA immunofluorescence.

(C) The surface expression of HA-hM4D^{nrxn} is distributed to the axonal compartment, as illustrated by a reduction in soma:axon (S/A) immunofluorescence ratio, relative to HA-hM4D.

(D) In cortical brain slices coexpressing hM4D^{nrxn} and ChR2, synaptic inhibition of L2/3 → L5 transmission is as effective with hM4D^{nrxn} (n = 5) as with hM4D (n = 8).

(E) The dose response relationship for synaptic inhibition with CNO is similar for hM4D^{nrxn} and hM4D.

(F) Hyperpolarization in L2/3 cortical neurons expressing hM4D^{nrxn} was negligible with CNO (1 μM) (n = 6).

(G) Conductance change in response to CNO (1 μM) is markedly reduced in L2/3 cortical neurons expressing hM4D^{nrxn} (n = 6), as compared to hM4D (n = 7). Values are represented as means ± SEM; n.s. $p > 0.05$, $^{**}p < 0.01$, $^{***}p < 0.001$.

relationship for CNO-mediated inhibition of ARC^{AGRP} → PVH projections, we identified 3 μM CNO as sufficient to induce maximal suppression of this circuit (Figure 3E) with a precision of ±500 μm. hM4D-mediated synaptic inhibition is therefore an efficacious and selective means of performing functional in vivo analysis of spatially defined axon projections from molecularly defined neuron populations.

Selective Synaptic Silencing with hM4D Axonal Targeting

In light of the dual properties of hM4D/CNO as a silencer of neuron electrical activity and synaptic vesicle release, we further refined hM4D for selective synaptic silencing by engineering an axon-selective variant. Preferential axonal distribution of membrane proteins has been accomplished by addition of amino acid sequences that bind myosin motors, which preferentially shuttle surface proteins into axons (Lewis et al., 2011). Alternatively, a membrane protein may be delivered to both somatodendritic and axonal compartments and then actively removed from the surface at the cell body by selective somatodendritic endocytosis, as has been shown for a member of the neurexin superfamily (Bel et al., 2009). Because the native human M4 receptor is already present at presynaptic terminals (Rouse et al., 1998), we chose to reduce somatic surface expression of hM4D, while maintaining axonal distribution, with the C-terminal addition of the intracellular sequence of neurexin 1α (Fairless et al., 2008; Kim et al., 2012) and a 2× hemagglutinin (HA) tag, resulting in the modified receptor hM4D^{nrxn} (Figure 4A).

To examine whether the subcellular distribution of hM4D^{nrxn} at the extracellular membrane surface is biased to axons, we also developed N-terminal-tagged hM4D variants with extracellular presentation of an HA epitope. Cell surface labeling of HA-hM4D

and HA-hM4D^{nrxn} (see Experimental Procedures) revealed reduced HA-hM4D^{nrxn} somatic expression, but axonal expression was maintained, which resulted in a reduced somatic:axonal (S/A) distribution for this receptor (S/A ratio, HA-hM4D: 0.88 ± 0.07; HA-hM4D^{nrxn}: 0.23 ± 0.03; $p < 0.001$, two-sample t test assuming unequal variance, n = 5 and 6, respectively) (Figures 4B and 4C). Synaptic silencing of L2/3 → L5 projections with hM4D^{nrxn} is robust (synaptic inhibition at 1 μM CNO: 92.6% ± 5.5%; n = 5) (Figures 4D and 4E). However, consistent with its largely axonal subcellular distribution, hM4D^{nrxn} activation in L2/3 cortical neurons with CNO lacks significant somatic hyperpolarization (V_m, baseline: −66.0 ± 2.3 mV; 1 μM CNO: −66.3 ± 2.2 mV; p = 0.3, paired t test, n = 6) (Figure 4F) and also lacks the somatic conductance increase seen with hM4D activation (ΔG_{in} at 1 μM CNO, hM4D: 23.0% ± 6.1%; hM4D^{nrxn}: 2.2% ± 1.4%; p = 0.007, two-sample t test assuming unequal variance, n = 7 and 6, respectively) (Figure 4G). This optimized tool allows selective and potent (Figure 4E) synaptic silencing with negligible effects on neuron excitability.

Selective Synaptic Silencing to Functionally Map a Hypothalamus → Brainstem Feeding Circuit In Vivo

To test the in vivo efficacy of the axon-selective synaptic silencing receptor, we applied hM4D^{nrxn} to functionally deconstruct an additional circuit node that regulates appetite. AGRP neuron activation results in feeding behavior, in part, by inhibition of PVH neurons, and, consistent with this, PVH neuron chemogenetic silencing with hM4D/CNO is sufficient to evoke food consumption (Figure S2A). Classic studies that used knife cuts and asymmetric "dual-disconnection" lesioning to produce overeating concluded that this behavior involved axon projections from PVH neurons to the nucleus of the solitary tract and dorsal vagal complex (NTS/DVC) in the hindbrain (Kirchgessner and Sclafani, 1988; McCabe et al., 1984). To further investigate the circuit node downstream of the PVH that is sufficient to elicit voracious food intake during loss-of-function manipulations, we sought to use cell-type-specific synaptic silencing of spatially defined PVH axon projections.

PVH neurons were selectively targeted in *Sim1-Cre* mice (a line with Cre-recombinase expression in the PVH) (Balthasar et al., 2005) by transduction with a Cre-dependent virus coexpressing hM4D^{nrxn} and the fluorescent protein mCherry. As with cortical neurons, activation of hM4D^{nrxn} with CNO in these PVH^{SIM1} neurons did not increase conductance, while hM4D/CNO did (ΔG_{in} at 1 μM CNO, hM4D: 24.8% ± 6.3%; hM4D^{nrxn}: 1.6% ± 0.9%; p = 0.007, two-sample t test assuming unequal variance, n = 6 and 8, respectively). As an initial test of efficacy, we confirmed that systemic CNO injection in mice with hM4D^{nrxn} in PVH^{SIM1} neurons, which should inhibit synaptic release from all of the axon projection fields of PVH neurons, was sufficient to evoke feeding (baseline feeding, 1 hr: 0.07 ± 0.01 g; CNO, 1 hr: 0.58 ± 0.02 g; n = 32). To functionally map PVH^{SIM1} axon projection fields that are involved in this hyperphagic behavior, we targeted intracranial CNO injections to PVH^{SIM1} axon projections in the hindbrain (Figures 5A and S3A). We first examined PVH^{SIM1} → NTS/DVC projections with bilateral delivery of CNO to the NTS/DVC in mice with hM4D^{nrxn} in PVH^{SIM1} neurons. This manipulation failed to significantly increase food intake, even with high dose CNO injections (baseline feeding, 1 hr: 0.07 ± 0.03 g; CNO 3, 300 μM: 0.1 ± 0.03 g; p = 0.3, paired t test, n = 9) (Figure 5B, far right). This was contrary to expectations based on knife cut and lesion experiments (Kirchgessner and Sclafani, 1988; McCabe et al., 1984), so we considered the possibility that a key excitatory serotonergic projection from raphe magnus/obscurus → NTS (Wu et al., 2012) may also have been lesioned in prior knife cut experiments but not in our cell-type-selective synaptic silencing experiments. NTS injection of the serotonin receptor 3 antagonist ondansetron has been used to block this circuit connection (Wu et al., 2012). However, hM4D^{nrxn}/CNO synaptic inhibition of PVH^{SIM1} → NTS/DVC in the presence of ondansetron (2 mM) was also insufficient to recapitulate the effects of systemic PVH^{SIM1} neuron silencing (baseline feeding, 1 hr: 0.12 ± 0.04 g; CNO 3, 30, or 300 μM: 0.06 ± 0.03 g; p = 0.2, paired t test, n = 6). Therefore, inhibition of PVH^{SIM1} → NTS/DVC axon projections is not sufficient to acutely elicit food consumption under these conditions.

To locate the circuit node responsible for feeding behavior during PVH neuron inhibition, we next used hM4D^{nrxn}/CNO to suppress synaptic release at several other hindbrain and midbrain sites targeted by PVH^{SIM1} axon projections. Based on in vivo dose response experiments in the ARC^{AGRP} → PVH circuit (Figure 3E), we used microinjection of 3 μM CNO to inhibit synaptic interactions at four additional positions along the neuraxis, which also included a range of sites along the transverse axis (Figure 5A). Under these conditions, we observed a functional "hotspot" that evoked feeding behavior during synaptic silencing of PVH^{SIM1} axons in the region of the caudal ventrolateral periaqueductal gray (PAGvl) and the dorsal raphe complex (DR) (baseline feeding, 1 hr: 0.09 ± 0.03 g; CNO: 0.49 ± 0.06 g, $p < 0.001$, paired t test, n = 10) (Figures 5B and 5C). Injections at more rostral locations were less effective at eliciting food intake with 3 μM CNO (Figures 5B and 5C; also see Figure S3B), further indicating that these behavioral effects of hM4D^{nrxn} activation were not due to inhibition of action potential transmission in axons of passage in vivo. Microinjections targeted to adjacent, caudal PVH^{SIM1} axon projections in the vicinity of the locus coeruleus and parabrachial nucleus only occasionally evoked feeding with 3 μM CNO (Figures 5B and 5C), typically requiring higher CNO concentrations (Figure 5D). Some midbrain and hindbrain intracranial microinjections had a trajectory that passed through a portion of the fourth cerebral ventricle, and injections targeted directly to either the cerebral aqueduct or the fourth ventricle could also evoke feeding in several cases (Figures S3Bi and S3Bii). However, this is not likely to be the cause of evoked feeding found for injections targeting the PAGvl/DR hotspot because (1) caudal injection sites usually exhibited extensive penetration of the fourth ventricle (sites in Figure 5C, far right), but none of these evoked food intake with 3 μM CNO; and (2) feeding could be elicited by intracranial injection of CNO (3 μM) around the PAGvl that did not damage the fourth ventricle (Figures S3Biii and S3Biv). Taken together, experiments using hM4D^{nrxn}/CNO for chemogenetic synaptic silencing identified the PAGvl/DR area as a key node downstream of the PVH that mediates feeding behavior.

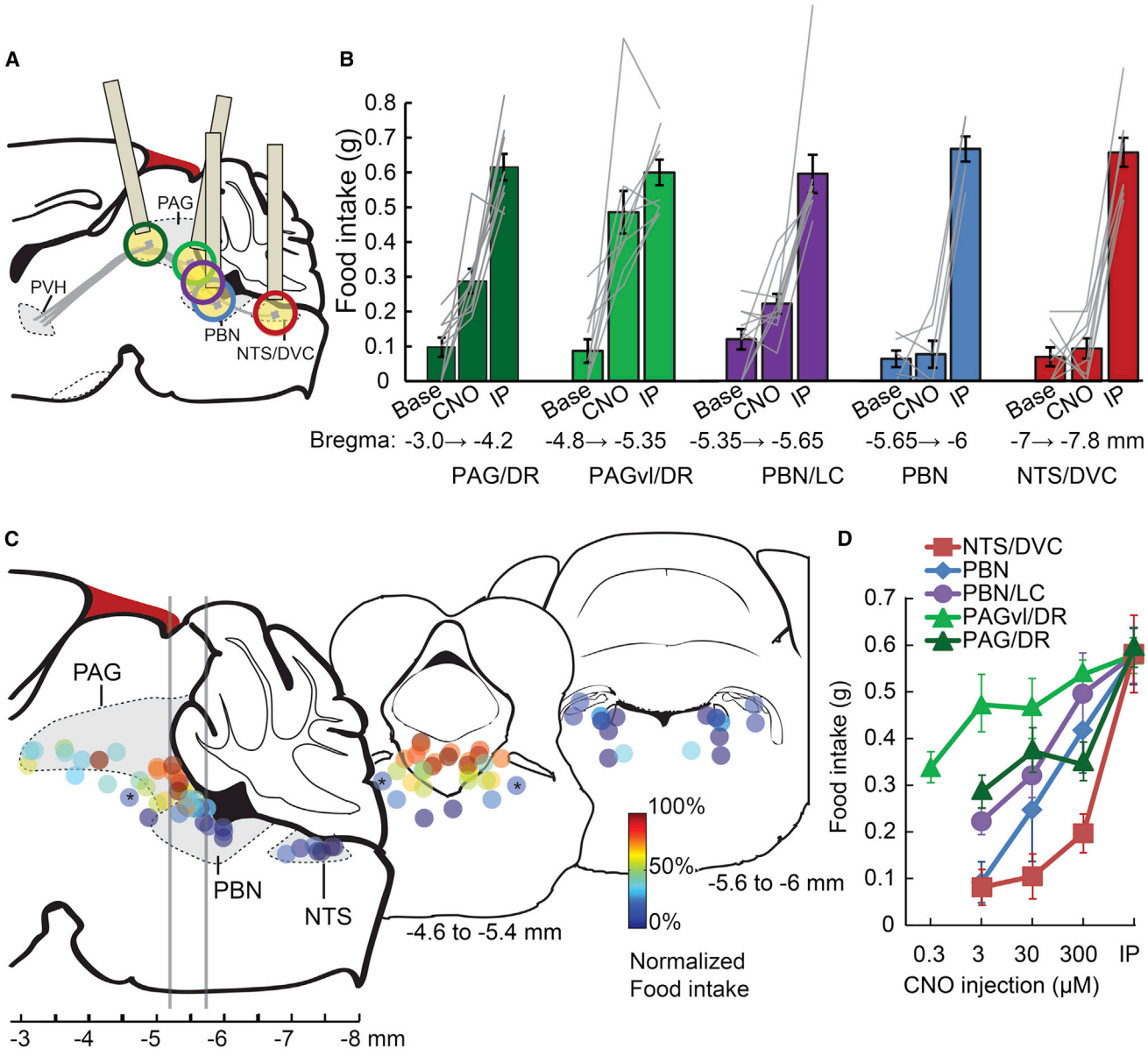

Figure 5. Cell-Type-Selective Synaptic Silencing Localizes a Feeding Circuit

(A) Schematic of descending axon projections from PVH^{SIM1} neurons, which express hM4D^{nrxn}. These axon projections were targeted in separate animals for spatially defined synaptic silencing by intracranial microinjection of CNO. Estimated precision of microinjections (based on ±500 μm) at each site is indicated by colored circles (for clarity, cannula schematic is not shown for "purple" injection site). Injection cannula was angled for PAG targeting in order to avoid the sinus confluens (blood vessel, dark red).

(B) Preinjection baseline (Base) and evoked feeding response (1 hr) from regions targeted by intracranial injections (CNO, 3 μM, typically bilateral) at distinct anterior-posterior positions. The most efficacious feeding responses were observed with microinjections into the PAGvl/DR (light green), which was similar to food consumption evoked by intraperitoneal injection of CNO (IP). Intracranial microinjections that were more ventral or dorsal than the indicated areas were not included in the analysis.

(C) Schematic of sagittal section showing the location of injection sites, which are color coded to reflect food intake evoked after intracranial 3 μM CNO microinjection, normalized to feeding after IP injection. Two transverse sections are displayed, at the level of PAGvl/DR and the caudal PBN, with the positions of multiple injection sites projected onto a coronal diagram. Bilateral injections are displayed as identically color-coded pairs. Asterisks denote bilateral microinjection site at the pedunculopontine tegmental nucleus (PPTg), which did not evoke substantial food intake.

(D) Dose response for CNO microinjections at different injection sites. Selectivity is reduced with increasing CNO dose, such that microinjection sites outside the PAGvl/DR region can evoke feeding. Values are represented as means ± SEM.

Table 1. Cell-Type-Specific Techniques for Silencing Axon Projections

Tool	Timescale	Mechanism	Limitations
NpHR/Arch	Millisecond to minutes	Inhibits action potential	Axons-of-passage also silenced
PSAM-GlyR	Minutes to 1 hr	Inhibits action potential	Axons-of-passage also silenced; intracranial microinjection
MIST	Minutes to hours	Inhibits transmitter release	Requires high expression level; intracranial microinjection
InSynC	Minutes to 1 day	Inhibits transmitter release	Increases spontaneous neurotransmitter release
hM4D^{nrxn}	Minutes to hours	Inhibits transmitter release	Intracranial microinjection

DISCUSSION

Chemogenetic Synaptic Silencing

Here, we describe a method to cell-type specifically silence neural circuit connections by inhibiting synaptic neurotransmitter release probability. hM4D^{nrxn}/CNO strongly suppresses neuronal output through synaptic inhibition without somatic hyperpolarization. Selective synaptic inhibition complements optogenetic (Stuber et al., 2011; Tye et al., 2011) or chemogenetic (Magnus et al., 2011) axonal silencing techniques, which can also block action potential transmission through axons of passage that target more distal brain areas. Therefore, selective synaptic silencing can enable a more precise localization of critical neural circuit interactions. Using ARC^{AGRP}→PVH, a previously characterized hypothalamic circuit interaction, to calibrate the in vivo dosing of CNO, we found that intracranial microinjection of 3 μM CNO is suitable for inhibiting synaptic interactions within ±500 μm of the injection site (Figure 3B). This calibration experiment was critical for determining the resolution for this system at an efficacious dose, and it also indicates better resolution here than a recent application of hM4D for projection silencing using microinjections of 1 mM CNO (Mahler et al., 2014). We also found a corresponding in vivo dose response relationship for CNO in synaptic silencing experiments with the axon-targeted variant hM4D^{nrxn} for the circuit PVH^{SIM1}→PAGvl/DR (Figure 5D), supporting the use of 3 μM CNO for intracranial microinjections. The precision of in vivo synaptic silencing for PVH^{SIM1}→PAGvl/DR could be further enhanced by tiling a region of interest with targeted CNO microinjections as demonstrated by the sharp hotspot we observed for evoked feeding behavior with microinjections at the midbrain/hindbrain boundary (Figures 5B and 5C). These results show that acute chemogenetic synaptic silencing can be used to localize circuit interactions that have a causal role for mouse behavior.

Using hM4D^{nrxn}/CNO, spatially defined synaptic output of molecularly defined neuron populations can be rapidly and selectively blocked, allowing the behavioral influence of a particular projection field to be examined. This approach offers an alternative to the commonly used method of pharmacological blockade of postsynaptic receptors, which undesirably impairs communication through other pathways and perturbs neuronal activity. Cell-type-selective hM4D/CNO synaptic silencing of the ARC^{AGRP}→PVH axonal release sites during exogenous AGRP neuron photostimulation tested the necessity of a specific projection field for feeding behavior and avoided unwanted alteration of baseline postsynaptic neuron activity. In addition, cell-type-selective synaptic silencing under endogenous neuronal activity patterns also can be used to functionally map behaviorally important circuit connections, which we applied to identify suppression of the PVH^{SIM1}→PAGvl/DR circuit connection as sufficient to induce overeating behavior.

Technical Considerations

Multiple methods are available for rapid, cell-type-specific and axon projection-selective inhibition of circuit function (Table 1). For rapid timescale silencing, optogenetic tools such as NpHR or Arch are necessary; however, for long-term projection silencing, these tools may require delivery of considerable energy into the brain. Optogenetic destruction of synaptic vesicle fusion machinery (InSynC) appears selective for silencing evoked release from specific synaptic targets, but this technique requires consideration of undesired elevated tonic spontaneous synaptic vesicle release (Lin et al., 2013). Our experiments indicate that chemogenetic silencing in vivo with hM4D or hM4D^{nrxn} and CNO robustly silences synaptic release within minutes, without significantly reducing axonal action potential propagation, and this reverses within 1–4 hr. In contrast, optogenetic activation of chloride or proton pumps (e.g., NpHR or Arch) (Jennings et al., 2013; Stuber et al., 2011) or the chemogenetic silencing tool PSAM-GlyR (Magnus et al., 2011) probably suppresses circuit connections by blocking action potential propagation (Tye et al., 2011), which, depending on axonal anatomy, can also influence axons of passage projecting to more distal brain areas. In our synaptic silencing experiments with PVH^{SIM1}→PAGvl/DR, we found that more rostral sites containing PVH axons were less effective at inducing overeating (Figures 5B and 5C), indicating that action potential propagation was not blocked. Therefore, synaptic silencing with hM4D^{nrxn} is well suited to disentangle the relative contribution of intermingled, molecularly defined axon projections at specific synaptic targets over timescales of minutes to hours.

The major limitation for using hM4D^{nrxn} to selectively silence synaptic projections involves the requirement to intracranially administer a CNO-containing solution. Pressure injections, which were used here, can diffuse and reduce resolution. In addition, pressure injections are not well suited to in vivo electrophysiological recordings due to tissue movement. An additional issue with intracranial microinjection is that it often requires perturbation of the animal's behavior during CNO infusion into the brain, which is unsuitable for some behavioral experiments. Finally, intracranial injections require consideration of the possible access of CNO into the ventricular system. In our experiments, this was potentially an issue; however, many of the injections following trajectories that passed through the fourth ventricle did not affect feeding, and some microinjections to

suppress PVH^{SIM1}→PAGvl/DR that resulted in overeating did not penetrate the fourth ventricle (Figure S3Biii). Because intracranial microinjections are widely used in behavioral studies, these considerations are well appreciated as are appropriate control experiments (as in Figure S3B).

Synaptic Silencing for Mapping a Feeding Circuit in the Mouse Brain

Our investigation of the circuits through which suppression of PVH neuron activity elicits feeding behavior was unable to confirm the prediction of classical lesion and knife cut experiments, which concluded that hyperphagia from PVH loss of function was mediated by a PVH→NTS/DVC circuit projection. Instead, we found that synaptic silencing of PVH^{SIM1} axon projections to the PAGvl/DR region elicited feeding. It is unlikely that the behavioral response resulted from spread of CNO to more caudal PVH^{SIM1} axonal release sites, such as the PBN or the locus coeruleus (Figure S3A), because direct injections into these areas did not elicit food intake with 3 μM CNO. PVH^{SIM1} axon projections to the pedunculopontine tegmental nucleus (PPTg) (Figure S3A) are also less likely to be directly responsible for feeding in these experiments, because direct targeting with 3 μM CNO failed to elicit feeding (asterisk in Figure 5C). Another nearby brain area, the lateral dorsal tegmental area (LDTg), had few PVH^{SIM1} axons (Figure S3A). Therefore, using the hM4D^{nrxn}/CNO synaptic silencing method indicates a PVH^{SIM1}→PAGvl/DR circuit that restrains appetite and is sufficient to mediate rapid food intake associated with PVH neuron inhibition, for example, by interoceptive AGRP neurons that read out circulating signals of bodily energy status (ARC^{AGRP}→PVH^{SIM1}→PAGvl/DR).

The circuit interaction from PVH to PAGvl/DR has been described anatomically (Geerling et al., 2010; Zheng et al., 1995), but the functional properties are not understood. Many PVH neurons express the vesicular glutamate transporter 2 (*Slc17a6*), but few PVH neurons express vesicular GABA transporter (Figure S3D). Furthermore, genetic deletion of *Slc17a6* from the PVH can lead to hyperphagia (Xu et al., 2013), indicating that PVH^{SIM1}→PAGvl/DR may be an excitatory circuit that suppresses appetite, and loss of function evokes feeding. Additionally, multiple neuropeptides present in different PVH populations could also influence the functional characteristics of this circuit. Although the role of the PAGvl to elicit feeding behavior is mostly unexamined, refeeding after food deprivation is suppressed by PAG microinjections of the neuropepide bombesin (Kyrkouli et al., 1987), and feeding during lateral hypothalamus electrical stimulation is inhibited by morphine in the PAGvl (Jenck et al., 1987). The DR has been implicated in feeding behavior using electrolytic lesions (Fletcher and Coscina, 1993) as well as inactivation of the DR with muscimol (Klitenick and Wirtshafter, 1988), both of which increased feeding in rats. DR is a major source of brain serotonin, which is a pathway targeted in clinical approaches to reduce food intake and body weight (Halford et al., 2011). The experiments reported here prioritize PAGvl and DR for more detailed analysis of the relative contribution of the component cell types downstream of PVH^{SIM1} neurons that control food intake.

Our experiments that did not find evidence for acute feeding control from silencing circuit connections from PVH^{SIM1}→NTS/DVC contrast with conclusions drawn from classical dual asymmetric lesion experiments. Those studies found that unilateral lesions of PVH and contralaterally positioned knife cuts around the NTS increased feeding dramatically, indicating a role for the NTS/DVC in PVH^{SIM1}-evoked feeding (Kirchgessner and Sclafani, 1988). In addition, PVH injection of noradrenaline results in feeding, and this was blocked with knife cuts in PAG, PBN, and ventral medulla, corresponding to the trajectory of descending PVH fibers (McCabe et al., 1984; Weiss and Leibowitz, 1985). Together with our experiments indicating a key PVH^{SIM1}→PAGvl/DR circuit, these results might reflect the possibility that caudal hindbrain knife cuts sever a further descending circuit originating from PAGvl/DR to regions in the vicinity of the NTS. Alternatively, because knife cuts and lesions do not distinguish ascending and descending axons, these manipulations might also have cut an ascending appetite suppression circuit (see, for example NTS→PBN [Wu et al., 2012]), which in concert with a unilateral PVH lesion could result in a feeding response. The complexity associated with interpretation of nonselective lesion methods for circuit functional analysis further highlights the usefulness of the genetically encoded, pharmacologically selective, and synapse-specific manipulations enabled by hM4D^{nrxn}/CNO silencing.

EXPERIMENTAL PROCEDURES

All experimental protocols were conducted according to U.S. National Institutes of Health guidelines for animal research and were approved by the Institutional Animal Care and Use Committee at Janelia Farm Research Campus.

Mice

Animals were housed on a 12 hr light (06:00)/dark (18:00) cycle with ad libitum access to water and mouse chow (PicoLab Rodent Diet 20, 5053 tablet, TestDiet), unless otherwise noted. *Agrp-IRES-Cre* (Tong et al., 2008) and *Sim1-Cre* (Balthasar et al., 2005) mice have been described previously. For characterizing in vivo and ex vivo dose responses, both male and female mice were used in cortical brain slice physiology (11–17 days old), hypothalamic brain slice physiology (6–10 weeks old), and photostimulation (6–10 weeks old) experiments (Figures 1, 2, and 3). Most mice in PVH^{SIM1} circuit mapping experiments (Figure 5) were male (49/51 animals). For in utero electroporations, timed pregnant female C57Bl/6NCrl mice were purchased from Charles River Laboratories and neurons in embryonic day 15.5 embryos were electroporated following pressure microinjection (Picospritzer) into the right lateral ventricle of a DNA mixture (0.5 μg/μl, approximately 200 nl), encoding the channel or receptor of interest and an EGFP marker. For all animal surgeries, postoperative analgesia was provided. Buprenorphine was administered intraperitoneally (0.1 mg/kg) along with ketoprofen administered subcutaneously (5 mg/kg).

Viral Vectors

rAAV2/1-CAG-FLEX-*rev*-ChR2tdTomato, rAAV-CAG-FLEX-*rev*-hM4D-2a-EGFP, and rAAV-CAG-FLEX-*rev*-PSAM^{L141F}-GlyR were described previously (Atasoy et al., 2008, 2012; Magnus et al., 2011). The rAAV2/9-CAG-FLEX-*rev*-ChR2-2a-hM4D vector was prepared by ligating ChR2 and hM4D with an intervening DNA fragment encoding a T2a amino acid sequence from *Thosea asigna* virus (EGRGSLLTCGDVEENPGP) (Donnelly et al., 2001), inserted into the rAAV2-CAG-FLEX backbone in an inverted orientation. Codon-optimized hM4D^{nrxn} (DNA 2.0) was constructed from hM4D with a C-terminal 2× HA tag and followed by the intracellular domain of neurexin-1α (aa 1,425–1,479). rAAV2/9-CAG-FLEX-*rev*-mCherry-2a-hM4D^{nrxn} was prepared by ligating mCherry and hM4D^{nrxn} with an intervening DNA fragment encoding a T2a amino acid sequence (EGRGSLLTCGDVEENPGP) and insertion into the rAAV2-CAG-FLEX backbone in an inverted orientation. Viral vectors were produced by the University of Pennsylvania Gene Therapy Program Vector Core or the Janelia Farm

Molecular Biology Core Facility. Plasmids developed for this study are available at http://www.addgene.org/Scott_Sternson/.

Viral Injections, Fiber, and Cannula Placement

Viral injections were performed as described previously (Atasoy et al., 2008) (postnatal days 21–25 [P21–P25] for electrophysiological recordings, P40–P50 for behavioral experiments). For AGRP neuron somatic activation in the ARC in conjunction with $ARC^{AGRP} \rightarrow$PVH synaptic inhibition, adult male and female *Agrp-IRES-Cre* animals were unilaterally transduced in the arcuate nucleus with rAAV2/9-CAG-FLEX-*rev*-ChR2-2a-hM4D or in a few cases rAAV-CAG-FLEX-*rev*-hM4D-2a-EGFP plus rAAV2/10-CAG-FLEX-*rev*-ChR2tdtomato (400 nl per side). ARC coordinates were the following: bregma −1.45 mm, midline +0.15 and +0.25 mm; dorsal surface −6.05 mm and −5.95 mm. For photostimulation experiments, a guide cannula was inserted ipsilaterally into the PVH (bregma −0.7 mm, midline 0.2 mm, dorsal surface −3.5 mm, 26 GA) and a ferrule-capped optical fiber was placed at an angle to target the ARC over the ChR2-transduced AGRP neurons (bregma −2.9, midline 0.15 mm, dorsal surface −4.65 mm, angled 13° toward anterior). CNO injection into AGRP neuron photostimulation control subjects lacking hM4D were *Agrp-IRES-Cre;Ai32* (Madisen et al., 2010) and *Agrp-IRES-Cre* animals unilaterally transduced in the arcuate nucleus with rAAV-CAG-FLEX-*rev*-$PSAM^{L141F}$-GlyR plus rAAV2/10-CAG-FLEX-*rev*-ChR2-tdtomato for 20 weeks. Higher AGRP neuron ChR2 penetrance and expression levels probably account for the increased evoked feeding observed in these animals relative to ChR2-2a-hM4D animals, which were used 4-6 weeks after rAAV injection.

For synaptic silencing of PVH axon projections, adult *Sim1-Cre* animals were bilaterally transduced in the PVH with rAAV2/9-CAG-FLEX-*rev*-mCherry-2a-$hM4D^{nrxn}$ or in a few cases rAAV-CAG-FLEX-*rev*-hM4D-2a-EGFP (300 nl per side). PVH coordinates were the following: bregma −0.7 mm; midline ±0.25 mm; dorsal surface −4.9 mm, −4.7 mm, and −4.5 mm. Animals well infected with either hM4D or $hM4D^{nrxn}$ reliably produced feeding after 2.5–3 weeks of expression. In mice that ate at least 0.4 g/hr in response to i.p. CNO, bilateral cannulas (26 GA) were then placed at various rostral-caudal positions, varying in lateral separation to match the trajectory of PVH^{SIM1} axon projections. Cannula position coordinates were the following: NTS/DVC cannula (bregma −7.2 mm, midline ±0.25 mm or ±0.5 mm, dorsal surface −4.2 mm); PBN cannula (bregma −5.8 mm, midline ±1 mm or ±1.5 mm, dorsal surface −3.7 mm); LC cannula (bregma −5.8 mm, midline ±0.25 mm or ±0.5 mm, dorsal surface −3.7 mm, angled 10° toward anterior); PAGvl/DR cannula (bregma −5.6 mm, midline ±0.25 mm or ±0.5 mm, dorsal surface −3.5 mm, angled 10°–14° toward anterior); PAG anterior (bregma −2.9 mm, midline ±0.5 mm, dorsal surface −3.2 mm, angled 0°–25° toward posterior); cerebral aqueduct (bregma −2.9 mm, midline 0 mm, dorsal surface −3.2 mm, angled 10°–12° toward posterior); fourth ventricle (bregma −5.8 mm, midline 0 mm, dorsal surface −3.7 mm). Injections targeting PAG were made at an angle to avoid rupturing the vasculature at the confluence of the superior sagittal sinus and transverse sinus (bregma −3.1 mm to −5.2 mm). Grip cement (DENTSPLY) was used to anchor the guide cannula and ferrule-capped fibers to the skull. Dummy cannulae (Plastics One) were inserted to keep the fiber guide from getting clogged. After surgery, mice were allowed 17–42 days for recovery and transgene expression. Bilateral intracranial injections were 50–100 nl/side. To determine dose response relationships for each injection site, we made repeated injections of CNO (0.3–300 μM) for each animal, separated by 2–3 days between trials.

In Vivo Photostimulation and Behavior

Components for food consumption monitoring and photostimulation were similar to those reported previously (Aponte et al., 2011). Light was delivered to the brain through an optical fiber (200-μm-diameter core; BFH48-200-Multimode, NA 0.48; Thorlabs) capped with 1.25 mm OD zirconia ferrules, implanted into the brain, and affixed to the skull of the animal with dental cement. For light delivery, the implanted ferrule-capped fiber was coupled to another optical fiber running to the fiber port with a matching 1.25 mm OD zirconium ferrule using a zirconium sleeve. The fiber tip was positioned to a distance of ~0.3 mm from the targeted region. For optical delivery of light pulses with millisecond precision to multiple mice, the output from a diode laser (473 nm, Altechna) was split into four beams using beam splitters (Fiber Sense and Signals). The main output beam from the diode laser was controlled using an acousto-optic modulator (Quanta Tech, OPTO-ELECTRONIC) to generate light pulses that were launched into separate fiber ports (Thorlabs) and their corresponding optical fibers. For all in vivo photostimulation experiments, the pulse protocol was 10 ms pulses, 20 pulses for 1 s, repeated every 4 s for 1 hr. The light power exiting the fiber tip was 10–15 mW. Mice were allowed ad libitum access to food overnight and, in the morning, were subjected to either 1 hr of photostimulation or injection with CNO. Reported food consumption amounts are totals over 1 hr.

Pharmacology

CNO (Enzo Life Sciences) and CNQX (20 μM; Sigma) were bath applied in aCSF with gravity perfusion. For cerebral microinjections, CNO was diluted in buffered saline containing 150 mM NaCl, 10 mM D-glucose, 10 mM HEPES, 2.5 mM KCl, 1 mM $MgCl_2$ (pH 7.35), 312 mOsm. Ondansetron HCl (0.6 mg/ml; Sigma) was dissolved in saline (Wu et al., 2012).

Electrophysiology

For details of ex vivo electrophysiology, see Supplemental Experimental Procedures.

Ex Vivo Circuit Mapping

For brain slice optogenetic experiments, we used laser-scanning photostimulation in which a laser (473 nm) was used to deliver a light as a focused spot (0.1–1 mW) to discrete positions on the specimen (Atasoy et al., 2008). Laser power was monitored with a photodiode. Light pulse duration (1–10 ms) was controlled by a Pockels cell and a mechanical shutter. A focused spot of light was targeted onto the specimen with two scanning mirrors through 4× or 63× objectives. Using a 4× objective, the light spot was moved along an 8 × 16 grid of photostimulation sites separated by 75 μm overlaid on the field of view (Petreanu et al., 2007), perpendicular to the cortical layers in cortical recordings or parallel to the third ventricle in hypothalamic recordings (Atasoy et al., 2008; Sternson et al., 2005). To assess how hM4D would influence action potential initiation, we made loose-seal cell-attached recordings (seal resistance, 20–100 MΩ, electrode resistance 4–8 MΩ, aCSF internal, voltage clamp) from transfected neurons in L2/3 or ARC. The average action potential response fidelity (action potentials/photostimulus) from the four photostimulation sites nearest the recorded cell was quantified before and during CNO perfusion. To assess orthodromic action potential propagation, we made axon-attached recordings (Atasoy et al., 2012) from the cut ends of L2/3 neuron transfected axons (identified by EGFP fluorescence) in layer 4 or layer 5. The average action potential fidelity was recorded in these axons during photostimulation of four sites in the center of L2/3 before and during CNO perfusion. For action potential backpropagation, loose-seal cell-attached recordings were made from transfected L2/3 cells, and the average action potential fidelity from photostimulation sites targeted to L5 was recorded before and during CNO perfusion. To assess light-evoked synaptic transmission in cortical slices, we made whole-cell voltage-clamp recordings from L5 neurons. Measurements of L5 synaptic charge and peak amplitude were drawn from a 4 × 4 or 5 × 5 set of photostimulation sites located in layer 2/3 and paired-pulse values were drawn from four sites in the center of this area. For synaptic analysis, peak amplitude is reported for simplicity, whereas statistical analysis was performed using synaptic charge transfer to account for possible changes in ChR2-evoked spike timing induced by hM4D-mediated hyperpolarization. Findings of statistical significance were not different between methods.

Hippocampal Neuronal Culture and Electroporation

To localize hM4D receptor present on the cell surface, we altered a tagged hM4D construct that expresses HA at the extracellular N terminus (HA-hM4D, Addgene ID 45548 [Armbruster et al., 2007]), by adding the C-terminal intracellular domain of neurexin-1α (aa 1,425–1,479, codon optimized, DNA 2.0) to the C terminus of HA-hM4D to produce $HA\text{-}hM4D^{nrxn}$. Cells were transfected with HA-hM4D or $HA\text{-}hM4D^{nrxn}$ DNA plus EGFP using the Nucleofector kit (LONZA) and AMAXA electroporation unit. For details about hippocampal neuronal culture, see Supplemental Experimental Procedures.

Immunohistochemistry and Imaging

After mice were used for behavioral experiments, they were transcardially perfused with 4% paraformaldehyde (PFA) 0.1 M phosphate buffer fixative. Tissue was postfixed in this solution for 4–12 hr and washed overnight in PBS (pH 7.4). Brain sections (50 μm) were processed for immunohistochemistry and mounted using VECTASHIELD. Microinjection experiments were confirmed by post hoc examination of the injection site with 100 nl of FluoroGold (Santa Cruz). Antibodies included anti-AGRP (1:5,000, goat, Neuronomics), anti-HA (1:3,000, rat, Roche), anti-tdTomato (1:20,000, guinea pig, Covance), and anti-EGFP (1:2,000, sheep, ABDSerotec). Fluorophore-conjugated secondary antibodies were from Jackson ImmunoResearch (1:500). Antibodies were diluted in PBS, 1% BSA, 0.1% Triton X-100.

For surface labeling, we used an anti-HA primary antibody, without permeabilization, in hippocampal neurons expressing HA-hM4D and HA-hM4D^{nrxn}. Neuronal cultures (6–20 DIV, 50,000 cells per dish) transfected with 0.5 ng EGFP and HA-hM4D or HA-hM4D^{nrxn} were fixed for 5 min in 4% PFA 4% sucrose in PBS, blocked with 3% normal goat serum for 30 min, incubated 15 min with anti-HA primary (1:3,000), 60 min with Alexa 594 secondary (1:500 in PBS), and mounted with Prolong Gold (Life Technologies). Images were collected by confocal microscopy (Zeiss 510, Zeiss 710, and Nikon A1R), using identical imaging conditions for both constructs. From the cell body of transfected neurons, the EGFP-labeled axon was followed until synaptic boutons could be identified. Soma:axon ratios (S/A) for hM4D and hM4D^{nrxn} were quantified using ImageJ. The average somatic HA-immunofluorescence intensity (minus average background intensity) was quantified from a single confocal plane by centering two orthogonal linescan cross-sections across the cell body of the surface-labeled neuron. To calculate S/A ratio, we compared the average pixel intensity from a 0.7-μm-wide region across the somatic cell membranes to the average HA-immunofluorescence intensity in the axon of the same neuron, quantified from four linescans across axonal boutons. As a negative control, cells transfected with EGFP alone were surface immunostained for HA.

Statistics

Values are represented as means ± SEM. p values for pairwise comparisons were calculated by Student's t test. IC_{50} calculation was in MATLAB. n.s. $p > 0.05$, *$p < 0.05$, **$p < 0.01$, ***$p < 0.001$.

ACCESSION NUMBERS

The GenBank accession number for the hM4D^{nrxn} sequence reported in this paper is KJ685217.

SUPPLEMENTAL INFORMATION

Supplemental Information includes Supplemental Experimental Procedures and three figures and can be found with this article online at http://dx.doi.org/10.1016/j.neuron.2014.04.008.

AUTHOR CONTRIBUTIONS

T.J.S, A.G., and S.M.S. designed experiments; T.J.S. performed the experiments; and T.J.S. and S.M.S. wrote the paper.

ACKNOWLEDGMENTS

This research was funded by the Howard Hughes Medical Institute. T.J.S. was funded by the HHMI Janelia Farm Visitor program. We thank A. Wardlaw, K. Morris, and S. Lindo for mouse breeding, genotyping, and viral injections; X. Zhang for molecular cloning; S. Michael for immunohistochemistry; B. Shields for cell culture; and D. Atasoy for contributive discussions and preliminary in vivo synaptic silencing experiments.

Accepted: March 27, 2014
Published: April 24, 2014

REFERENCES

Aponte, Y., Atasoy, D., and Sternson, S.M. (2011). AGRP neurons are sufficient to orchestrate feeding behavior rapidly and without training. Nat. Neurosci. *14*, 351–355.

Armbruster, B.N., Li, X., Pausch, M.H., Herlitze, S., and Roth, B.L. (2007). Evolving the lock to fit the key to create a family of G protein-coupled receptors potently activated by an inert ligand. Proc. Natl. Acad. Sci. USA *104*, 5163–5168.

Atasoy, D., Aponte, Y., Su, H.H., and Sternson, S.M. (2008). A FLEX switch targets Channelrhodopsin-2 to multiple cell types for imaging and long-range circuit mapping. J. Neurosci. *28*, 7025–7030.

Atasoy, D., Betley, J.N., Su, H.H., and Sternson, S.M. (2012). Deconstruction of a neural circuit for hunger. Nature *488*, 172–177.

Balthasar, N., Dalgaard, L.T., Lee, C.E., Yu, J., Funahashi, H., Williams, T., Ferreira, M., Tang, V., McGovern, R.A., Kenny, C.D., et al. (2005). Divergence of melanocortin pathways in the control of food intake and energy expenditure. Cell *123*, 493–505.

Bel, C., Oguievetskaia, K., Pitaval, C., Goutebroze, L., and Faivre-Sarrailh, C. (2009). Axonal targeting of Caspr2 in hippocampal neurons via selective somatodendritic endocytosis. J. Cell Sci. *122*, 3403–3413.

Blackmer, T., Larsen, E.C., Takahashi, M., Martin, T.F., Alford, S., and Hamm, H.E. (2001). G protein betagamma subunit-mediated presynaptic inhibition: regulation of exocytotic fusion downstream of Ca2+ entry. Science *292*, 293–297.

Bock, R., Shin, J.H., Kaplan, A.R., Dobi, A., Markey, E., Kramer, P.F., Gremel, C.M., Christensen, C.H., Adrover, M.F., and Alvarez, V.A. (2013). Strengthening the accumbal indirect pathway promotes resilience to compulsive cocaine use. Nat. Neurosci. *16*, 632–638.

de Jong, A.P., and Verhage, M. (2009). Presynaptic signal transduction pathways that modulate synaptic transmission. Curr. Opin. Neurobiol. *19*, 245–253.

Dittman, J.S., and Regehr, W.G. (1996). Contributions of calcium-dependent and calcium-independent mechanisms to presynaptic inhibition at a cerebellar synapse. J. Neurosci. *16*, 1623–1633.

Dobrunz, L.E., and Stevens, C.F. (1997). Heterogeneity of release probability, facilitation, and depletion at central synapses. Neuron *18*, 995–1008.

Dolezal, V., and Tucek, S. (1998). The effects of brucine and alcuronium on the inhibition of [3H]acetylcholine release from rat striatum by muscarinic receptor agonists. Br. J. Pharmacol. *124*, 1213–1218.

Donnelly, M.L., Hughes, L.E., Luke, G., Mendoza, H., ten Dam, E., Gani, D., and Ryan, M.D. (2001). The 'cleavage' activities of foot-and-mouth disease virus 2A site-directed mutants and naturally occurring '2A-like' sequences. J. Gen. Virol. *82*, 1027–1041.

Fairless, R., Masius, H., Rohlmann, A., Heupel, K., Ahmad, M., Reissner, C., Dresbach, T., and Missler, M. (2008). Polarized targeting of neurexins to synapses is regulated by their C-terminal sequences. J. Neurosci. *28*, 12969–12981.

Fletcher, P.J., and Coscina, D.V. (1993). Injecting 5-HT into the PVN does not prevent feeding induced by injecting 8-OH-DPAT into the raphe. Pharmacol. Biochem. Behav. *46*, 487–491.

Geerling, J.C., Shin, J.W., Chimenti, P.C., and Loewy, A.D. (2010). Paraventricular hypothalamic nucleus: axonal projections to the brainstem. J. Comp. Neurol. *518*, 1460–1499.

Halford, J.C., Boyland, E.J., Lawton, C.L., Blundell, J.E., and Harrold, J.A. (2011). Serotonergic anti-obesity agents: past experience and future prospects. Drugs *71*, 2247–2255.

Heinke, B., Gingl, E., and Sandkühler, J. (2011). Multiple targets of μ-opioid receptor-mediated presynaptic inhibition at primary afferent Aδ- and C-fibers. J. Neurosci. *31*, 1313–1322.

Hescheler, J., Rosenthal, W., Trautwein, W., and Schultz, G. (1987). The GTP-binding protein, Go, regulates neuronal calcium channels. Nature *325*, 445–447.

Jenck, F., Quirion, R., and Wise, R.A. (1987). Opioid receptor subtypes associated with ventral tegmental facilitation and periaqueductal gray inhibition of feeding. Brain Res. *423*, 39–44.

Jennings, J.H., Rizzi, G., Stamatakis, A.M., Ung, R.L., and Stuber, G.D. (2013). The inhibitory circuit architecture of the lateral hypothalamus orchestrates feeding. Science *341*, 1517–1521.

Karpova, A.Y., Tervo, D.G., Gray, N.W., and Svoboda, K. (2005). Rapid and reversible chemical inactivation of synaptic transmission in genetically targeted neurons. Neuron *48*, 727–735.

Kim, J., Zhao, T., Petralia, R.S., Yu, Y., Peng, H., Myers, E., and Magee, J.C. (2012). mGRASP enables mapping mammalian synaptic connectivity with light microscopy. Nat. Methods *9*, 96–102.

Kirchgessner, A.L., and Sclafani, A. (1988). PVN-hindbrain pathway involved in the hypothalamic hyperphagia-obesity syndrome. Physiol. Behav. *42*, 517–528.

Kitamoto, T. (2002). Targeted expression of temperature-sensitive dynamin to study neural mechanisms of complex behavior in Drosophila. J. Neurogenet. *16*, 205–228.

Klitenick, M.A., and Wirtshafter, D. (1988). Comparative studies of the ingestive behaviors produced by microinjections of muscimol into the midbrain raphe nuclei of the ventral tegmental area of the rat. Life Sci. *42*, 775–782.

Krashes, M.J., Koda, S., Ye, C., Rogan, S.C., Adams, A.C., Cusher, D.S., Maratos-Flier, E., Roth, B.L., and Lowell, B.B. (2011). Rapid, reversible activation of AgRP neurons drives feeding behavior in mice. J. Clin. Invest. *121*, 1424–1428.

Kyrkouli, S.E., Stanley, B.G., and Leibowitz, S.F. (1987). Bombesin-induced anorexia: sites of action in the rat brain. Peptides *8*, 237–241.

Lewis, T.L., Jr., Mao, T., and Arnold, D.B. (2011). A role for myosin VI in the localization of axonal proteins. PLoS Biol. *9*, e1001021.

Lin, J.Y., Sann, S.B., Zhou, K., Nabavi, S., Proulx, C.D., Malinow, R., Jin, Y., and Tsien, R.Y. (2013). Optogenetic inhibition of synaptic release with chromophore-assisted light inactivation (CALI). Neuron *79*, 241–253.

Madisen, L., Zwingman, T.A., Sunkin, S.M., Oh, S.W., Zariwala, H.A., Gu, H., Ng, L.L., Palmiter, R.D., Hawrylycz, M.J., Jones, A.R., et al. (2010). A robust and high-throughput Cre reporting and characterization system for the whole mouse brain. Nat. Neurosci. *13*, 133–140.

Magnus, C.J., Lee, P.H., Atasoy, D., Su, H.H., Looger, L.L., and Sternson, S.M. (2011). Chemical and genetic engineering of selective ion channel-ligand interactions. Science *333*, 1292–1296.

Mahler, S.V., Vazey, E.M., Beckley, J.T., Keistler, C.R., McGlinchey, E.M., Kaufling, J., Wilson, S.P., Deisseroth, K., Woodward, J.J., and Aston-Jones, G. (2014). Designer receptors show role for ventral pallidum input to ventral tegmental area in cocaine seeking. Nat. Neurosci. *17*, 577–585.

McCabe, J.T., DeBellis, M., and Leibowitz, S.F. (1984). Clonidine-induced feeding: analysis of central sites of action and fiber projections mediating this response. Brain Res. *309*, 85–104.

Petreanu, L., Huber, D., Sobczyk, A., and Svoboda, K. (2007). Channelrhodopsin-2-assisted circuit mapping of long-range callosal projections. Nat. Neurosci. *10*, 663–668.

Photowala, H., Blackmer, T., Schwartz, E., Hamm, H.E., and Alford, S. (2006). G protein betagamma-subunits activated by serotonin mediate presynaptic inhibition by regulating vesicle fusion properties. Proc. Natl. Acad. Sci. USA *103*, 4281–4286.

Rouse, S.T., Gilmor, M.L., and Levey, A.I. (1998). Differential presynaptic and postsynaptic expression of m1-m4 muscarinic acetylcholine receptors at the perforant pathway/granule cell synapse. Neuroscience *86*, 221–232.

Sternson, S.M., Shepherd, G.M., and Friedman, J.M. (2005). Topographic mapping of VMH —> arcuate nucleus microcircuits and their reorganization by fasting. Nat. Neurosci. *8*, 1356–1363.

Stuber, G.D., Sparta, D.R., Stamatakis, A.M., van Leeuwen, W.A., Hardjoprajitno, J.E., Cho, S., Tye, K.M., Kempadoo, K.A., Zhang, F., Deisseroth, K., and Bonci, A. (2011). Excitatory transmission from the amygdala to nucleus accumbens facilitates reward seeking. Nature *475*, 377–380.

Takahashi, T., Kajikawa, Y., and Tsujimoto, T. (1998). G-Protein-coupled modulation of presynaptic calcium currents and transmitter release by a GABAB receptor. J. Neurosci. *18*, 3138–3146.

Tong, Q., Ye, C.P., Jones, J.E., Elmquist, J.K., and Lowell, B.B. (2008). Synaptic release of GABA by AgRP neurons is required for normal regulation of energy balance. Nat. Neurosci. *11*, 998–1000.

Tye, K.M., Prakash, R., Kim, S.Y., Fenno, L.E., Grosenick, L., Zarabi, H., Thompson, K.R., Gradinaru, V., Ramakrishnan, C., and Deisseroth, K. (2011). Amygdala circuitry mediating reversible and bidirectional control of anxiety. Nature *471*, 358–362.

Weiss, G.F., and Leibowitz, S.F. (1985). Efferent projections from the paraventricular nucleus mediating alpha 2-noradrenergic feeding. Brain Res. *347*, 225–238.

Wu, Q., Clark, M.S., and Palmiter, R.D. (2012). Deciphering a neuronal circuit that mediates appetite. Nature *483*, 594–597.

Xu, Y., Wu, Z., Sun, H., Zhu, Y., Kim, E.R., Lowell, B.B., Arenkiel, B.R., Xu, Y., and Tong, Q. (2013). Glutamate mediates the function of melanocortin receptor 4 on Sim1 neurons in body weight regulation. Cell Metab. *18*, 860–870.

Yamamoto, M., Wada, N., Kitabatake, Y., Watanabe, D., Anzai, M., Yokoyama, M., Teranishi, Y., and Nakanishi, S. (2003). Reversible suppression of glutamatergic neurotransmission of cerebellar granule cells in vivo by genetically manipulated expression of tetanus neurotoxin light chain. J. Neurosci. *23*, 6759–6767.

Zhang, W., Basile, A.S., Gomeza, J., Volpicelli, L.A., Levey, A.I., and Wess, J. (2002). Characterization of central inhibitory muscarinic autoreceptors by the use of muscarinic acetylcholine receptor knock-out mice. J. Neurosci. *22*, 1709–1717.

Zheng, J.Q., Seki, M., Hayakawa, T., Ito, H., and Zyo, K. (1995). Descending projections from the paraventricular hypothalamic nucleus to the spinal cord: anterograde tracing study in the rat. Okajimas Folia Anat. Jpn. *72*, 119–135.

Zucker, R.S., and Regehr, W.G. (2002). Short-term synaptic plasticity. Annu. Rev. Physiol. *64*, 355–405.